Best Spatial Distributions of Shell Kinematics Over 2D Meshes for Free Vibration Analyses

Noname manuscript No.
(will be inserted by the editor)

Best spatial distributions of shell kinematics over 2D meshes for free vibration analyses

Marco Petrolo · Erasmo Carrera

Received: date / Accepted: date

Abstract This paper proposes a novel approach to build refined shell models. The focus is on the free vibrations of composite panels, and the node-dependent-kinematics is used to select shell theories node-wise. The methodology shown in this work can provide at least two sets of information. First, it optimizes the use of shell models by indicating the minimum number of refined models to use. Then, it highlights which areas of the structures are more vulnerable to non-classical effects. Moreover, by varying various problem features, e.g., boundary conditions, thickness, and stacking sequence, the influence of those parameters on the modelling strategy is evaluated. The results suggest the predominant influence of thickness and boundary conditions and the possibility to improve the quality of the solution via the proper use of the refinement strategy.

Keywords Shell · Finite Element Method · Node Dependent Kinematics

1 Introduction

Shell theories depend on variable distributions along the thickness direction, and such distributions define the number of degrees of freedom (DOF) per node. Shell elements in commercial codes rely on the classical theories of structures [1–6] and the maximum number of DOF is six, namely, three displacements and rotations. Classical models are reliable if the structure is thin,

M. Petrolo
MUL2 Group, Department of Mechanical and Aerospace Engineering
Tel.: +39-011-090-6845
E-mail: marco.petrolo@polito.it

E. Carrera
MUL2 Group, Department of Mechanical and Aerospace Engineering
Tel.: +39-011-090-6836
E-mail: erasmo.carrera@polito.it

there are no local effects, and in-plane stress and transverse displacements are of interest. Concerning composite structures, several phenomena fall beyond the prediction capabilities of classical models [7,8]. Examples are high transverse deformability and anisotropy, edge-effects, local distortions, higher-order oscillations, cracks, and contacts as transverse stresses and normal stretch become primarily important. Other examples of critical problems are those with multifield interactions such as thermal problems in which the material characteristics can change significantly and in an anisotropic manner.
The improvement of classical models has to consider shear and normal transverse stresses, and variations of the displacement field at the interface between two layers with different mechanical properties, i.e., the zig-zag effect [9–20]. As a general guideline, the Koiter recommendations, i.e., the inclusion of both transverse shear and axial stress in refined theories, remain a valuable guideline that should lead the development of shell theories [11,21,22].
The present paper deals with the free vibration analysis of composite shells via FEM. In the last decades, many contributions have been published concerning this topic as shown by Qatu's comprehensive reviews [23,24]. A brief overview of works focused on the free vibration analysis via shells follows.
Many efforts focused on the development of exact, analytical or semi-analytical solutions to verify numerical approaches. Leissa and Reddy are among the main contributors with special attention paid to 3D solutions and shear deformation theories [14,25,26]. More recent contributions are in [27–33]. The extension of exact solutions to wider cases focused on general boundary conditions and laminations [34–40], shells with cutouts [41], conical shape geometries [42], stiffened and damaged structures [43], and non-homogeneous properties [44].
Other solution schemes make use of various approaches. An example is the Galerkin method for higher-order models [45,46], with mixed models based on the Reissner mixed variational method (RMVT) [47], and for conical shapes [48]. Another common solution is the Ritz and Rayleigh-Ritz with contributions on local boundary conditions [49,50], arbitrary boundary conditions and complex shapes [51–55], 3D-like models [56,57], sandwich structures [58], and comparisons with experimental results [59]. Other approaches are the spectral method for arbitrary boundary conditions and shapes [60], domain decomposition method [61–63], and the differential quadrature method [64].
The finite element method (FEM) has a great variety of contributions starting from early works a few decades ago [65–67]. Then, research focused on the element type, i.e., four- [68–70], eight- [71,72], and nine-node elements [73,74]. and the the order of the structural model [75–78]. Recent works have tried to improve numerical solutions via various approaches, such as assumed strain finite elements (FE) [79], wave finite element and wave based method [80,81], Haar wavelet method [82,83], spline collocation and convolution method [84–86], and the reverberation ray matrix [87].
Concerning the development of the structural theories, some of the most important strategies rely on the use of higher-order models [88–93], layer-wise models [94–98], and zig-zag [99]. Most of the contributions mentioned so far

exploit the axiomatic approach in which assumptions on the mechanical behavior of shells lead to the definition of the mathematical model along the thickness. A mathematically more rigorous approach is the asymptotic one that can provide the accuracy of a structural theory with respect to the 3D solution [100,101].
As mentioned above, the use of refined models is an attempt to tackle several mechanical phenomena. Given a structural problem, the spatial distribution of such phenomena can vary significantly and, usually, are more severe in the proximity of geometrical and mechanical boundary conditions. The necessity to use refined models in an area of the structure signals the presence of non-classical effects. This paper presents a novel strategy to evaluate the best distributions of shell theories over a 2D mesh, and, therefore, to determine the most critical area to model. The proposed methodology exploits the synergies between the Carrera Unified Formulation (CUF), the Node-Dependent-Kinematics (NDK) and the Axiomatic-Asymptotic-Method (AAM). CUF [102] is the theoretical framework providing the governing equations for all the structural models, independently of the order of the theory or the completeness of the expansions. Within CUF, one of the latest developments is NDK in which each node of an FE model can assume a different shell theory [103,104]. AAM [105,106] is a method to evaluate the accuracy of any-order shell model. The AAM leads to the best Theory Diagram (BTD) [107,108]. The BTD is a 2D plot to localize a shell model via its nodal degrees of freedom and accuracy. In the past, AAM results on structural dynamics focused on beam and shell finite elements [109,22]. The novelty of this paper stems from the evaluation of spatial distributions of shell theories. In other words, given a problem and a 2D mesh, the most convenient structural theory for each node is evaluated. In other words, this paper extends the methodology from [22] by introducing the possibility of changing the structural theory at the element level.
This paper is organized as follows: the governing equations and the methodology are in Sections 2 and 3; results in Section 4, and conclusions in Section 5.

2 Carrera Unified Formulation

Using the reference frame in Fig. 1, the CUF displacement field for a 2D model is

$$\mathbf{u}(\alpha,\beta,z) = F_\tau(z)\mathbf{u}_\tau(\alpha,\beta) \qquad \tau = 1,\dots,M \tag{1}$$

The Einstein notation acts on τ. F_τ are the thickness expansion functions. $\mathbf{u}_\tau$ is the vector of the generalized unknown displacements. M is the number of expansion terms. In the case of polynomial, Taylor-like expansions, a fourth-order model, referred to as N=4, has the following displacement field:

$$\begin{aligned} u_\alpha &= u_{\alpha_1} + z\,u_{\alpha_2} + z^2\,u_{\alpha_3} + z^3\,u_{\alpha_4} + z^4\,u_{\alpha_5} \\ u_\beta &= u_{\beta_1} + z\,u_{\beta_2} + z^2\,u_{\beta_3} + z^3\,u_{\beta_4} + z^4\,u_{\beta_5} \\ u_z &= u_{z_1} + z\,u_{z_2} + z^2\,u_{z_3} + z^3\,u_{z_4} + z^4\,u_{z_5} \end{aligned} \tag{2}$$

Fig. 1 Shell geometry

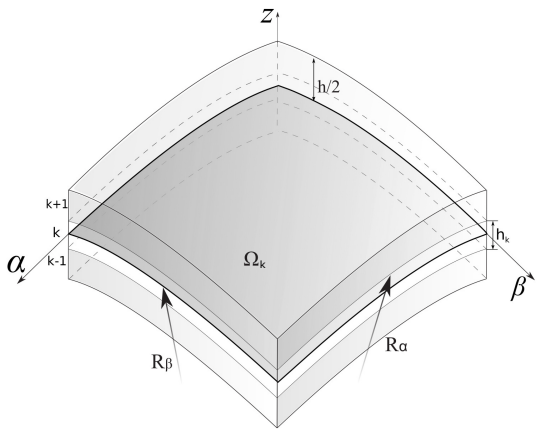

N=4 has fifteen nodal DOF. The order and type of expansion is a free parameter. Thus, the structure of the theory is an input of the analysis. The metric coefficients H^k_α, H^k_β and H^k_z of the k^{th} layer are

$$H^k_\alpha = A^k(1 + z_k/R^k_\alpha), \quad H^k_\beta = B^k(1 + z_k/R^k_\beta), \quad H^k_z = 1 \tag{3}$$

R^k_α and R^k_β are the principal radii of the middle surface of the k^{th} layer, A^k and B^k the coefficients of the first fundamental form of Ω_k, see Fig. 1. This paper focuses only on shells with constant radii of curvature with $\mathrm{A}^k = \mathrm{B}^k = 1$. The geometrical relations are

$$\begin{aligned} \boldsymbol{\epsilon}^k_p &= \left\{\epsilon^k_{\alpha\alpha}, \epsilon^k_{\beta\beta}, \epsilon^k_{\alpha\beta}\right\}^T = (\boldsymbol{D}^k_p + \boldsymbol{A}^k_p)\boldsymbol{u}^k \\ \boldsymbol{\epsilon}^k_n &= \left\{\epsilon^k_{\alpha z}, \epsilon^k_{\beta z}, \epsilon^k_{zz}\right\}^T = (\boldsymbol{D}^k_{n\Omega} + \boldsymbol{D}^k_{nz} - \boldsymbol{A}^k_n)\boldsymbol{u}^k \end{aligned} \tag{4}$$

where

$$\boldsymbol{D}^k_p = \begin{bmatrix} \frac{\partial_\alpha}{H^k_\alpha} & 0 & 0 \\ 0 & \frac{\partial_\beta}{H^k_\beta} & 0 \\ \frac{\partial_\beta}{H^k_\beta} & \frac{\partial_\alpha}{H^k_\alpha} & 0 \end{bmatrix} \quad \boldsymbol{D}^k_{n\Omega} = \begin{bmatrix} 0 & 0 & \frac{\partial_\alpha}{H^k_\alpha} \\ 0 & 0 & \frac{\partial_\beta}{H^k_\beta} \\ 0 & 0 & 0 \end{bmatrix} \quad \boldsymbol{D}^k_{nz} = \begin{bmatrix} \partial_z & 0 & 0 \\ 0 & \partial_z & 0 \\ 0 & 0 & \partial_z \end{bmatrix} \tag{5}$$

$$\boldsymbol{A}^k_p = \begin{bmatrix} 0 & 0 & \frac{1}{H^k_\alpha R^k_\alpha} \\ 0 & 0 & \frac{1}{H^k_\beta R^k_\beta} \\ 0 & 0 & 0 \end{bmatrix} \quad \boldsymbol{A}^k_n = \begin{bmatrix} \frac{1}{H^k_\alpha R^k_\alpha} & 0 & 0 \\ 0 & \frac{1}{H^k_\beta R^k_\beta} & 0 \\ 0 & 0 & 0 \end{bmatrix} \tag{6}$$

The stress-strain relations are

$$\begin{aligned} \boldsymbol{\sigma}^k_p &= \left\{\sigma^k_{\alpha\alpha}, \sigma^k_{\beta\beta}, \sigma^k_{\alpha\beta}\right\}^T = \boldsymbol{C}^k_{pp}\boldsymbol{\epsilon}^k_p + \boldsymbol{C}^k_{pn}\boldsymbol{\epsilon}^k_n \\ \boldsymbol{\sigma}^k_n &= \left\{\sigma^k_{\alpha z}, \sigma^k_{\beta z}, \sigma^k_{zz}\right\}^T = \boldsymbol{C}^k_{np}\boldsymbol{\epsilon}^k_p + \boldsymbol{C}^k_{nn}\boldsymbol{\epsilon}^k_n \end{aligned} \tag{7}$$

where

$$\begin{aligned} \boldsymbol{C}_{pp}^{k} &= \begin{bmatrix} C_{11}^{k} & C_{12}^{k} & C_{16}^{k} \\ C_{12}^{k} & C_{22}^{k} & C_{26}^{k} \\ C_{16}^{k} & C_{26}^{k} & C_{66}^{k} \end{bmatrix} \qquad \boldsymbol{C}_{pn}^{k} = \begin{bmatrix} 0 & 0 & C_{13}^{k} \\ 0 & 0 & C_{23}^{k} \\ 0 & 0 & C_{36}^{k} \end{bmatrix} \\ \boldsymbol{C}_{np}^{k} &= \begin{bmatrix} 0 & 0 & 0 \\ 0 & 0 & 0 \\ C_{13}^{k} & C_{23}^{k} & C_{36}^{k} \end{bmatrix} \qquad \boldsymbol{C}_{nn}^{k} = \begin{bmatrix} C_{55}^{k} & C_{45}^{k} & 0 \\ C_{45}^{k} & C_{44}^{k} & 0 \\ 0 & 0 & C_{33}^{k} \end{bmatrix} \end{aligned} \tag{8}$$

Where the orthotropic material coefficients are obtainable from nine independent coefficients, namely the Young and shear moduli, and Poisson ratios [110]. The FEM formulation adopts a nine-node shell element based on the Mixed Interpolation of Tensorial Component (MITC) method [111]. The displacement vector becomes

$$\delta \boldsymbol{u}_s = N_j \delta \boldsymbol{u}_{sj}, \qquad \boldsymbol{u}_\tau = N_i \boldsymbol{u}_{\tau i} \qquad i, j = 1, \cdots, 9 \tag{9}$$

$\boldsymbol{u}_{\tau i}$ and $\delta \boldsymbol{u}_{sj}$ are the nodal displacement vector and the virtual displacement, respectively. The strain expression becomes

$$\begin{aligned} \boldsymbol{\epsilon}_p &= F_\tau (\boldsymbol{D}_p + \boldsymbol{A}_p) N_i \boldsymbol{u}_{\tau i} \\ \boldsymbol{\epsilon}_n &= F_\tau (\boldsymbol{D}_{n\Omega} - \boldsymbol{A}_n) N_i \boldsymbol{u}_{\tau i} + F_{\tau_{,z}} N_i \boldsymbol{u}_{\tau i} \end{aligned} \tag{10}$$

MITC avoids the membrane and shear locking via a specific interpolation strategy for the strain components on the nine-node shell element, as follows:

$$\begin{aligned} \boldsymbol{\epsilon}_p &= \begin{bmatrix} \epsilon_{\alpha\alpha} \\ \epsilon_{\beta\beta} \\ \epsilon_{\alpha\beta} \end{bmatrix} = \begin{bmatrix} N_{m1} & 0 & 0 \\ 0 & N_{m2} & 0 \\ 0 & 0 & N_{m3} \end{bmatrix} \begin{bmatrix} \epsilon_{\alpha\alpha_{m1}} \\ \epsilon_{\beta\beta_{m2}} \\ \epsilon_{\alpha\beta_{m3}} \end{bmatrix} \\ \boldsymbol{\epsilon}_n &= \begin{bmatrix} \epsilon_{\alpha z} \\ \epsilon_{\beta z} \\ \epsilon_{zz} \end{bmatrix} = \begin{bmatrix} N_{m1} & 0 & 0 \\ 0 & N_{m2} & 0 \\ 0 & 0 & 1 \end{bmatrix} \begin{bmatrix} \epsilon_{\alpha z_{m1}} \\ \epsilon_{\beta z_{m2}} \\ \epsilon_{z z_{m3}} \end{bmatrix} \end{aligned} \tag{11}$$

Strains $\epsilon_{\alpha\alpha_{m1}}$, $\epsilon_{\beta\beta_{m2}}$, $\epsilon_{\alpha\beta_{m3}}$, $\epsilon_{\alpha z_{m1}}$, and $\epsilon_{\beta z_{m2}}$ result from Eq. 10 and

$$\begin{aligned} N_{m1} &= [N_{A1}, N_{B1}, N_{C1}, N_{D1}, N_{E1}, N_{F1}] \\ N_{m2} &= [N_{A2}, N_{B2}, N_{C2}, N_{D2}, N_{E2}, N_{F2}] \\ N_{m3} &= [N_P, N_Q, N_R, N_S] \end{aligned} \tag{12}$$

Subscripts m1, m2 and m3 indicate the point groups (A1,B1,C1,D1,E1,F1), (A2,B2,C2,D2,E2,F2), and (P,Q,R,S), respectively, see Fig. 2.
According to the Principle of Virtual Displacements (PVD),

$$\int_{\Omega_k} \int_{A_k} \delta {\boldsymbol{\epsilon}^k}^T \boldsymbol{\sigma}^k H_\alpha^k H_\beta^k d\Omega_k dz + \int_{\Omega_k} \int_{A_k} \rho^k \delta {\boldsymbol{u}^k}^T \ddot{\boldsymbol{u}}^k H_\alpha^k H_\beta^k d\Omega_k dz = 0 \tag{13}$$

Fig. 2 MITC9 tying points

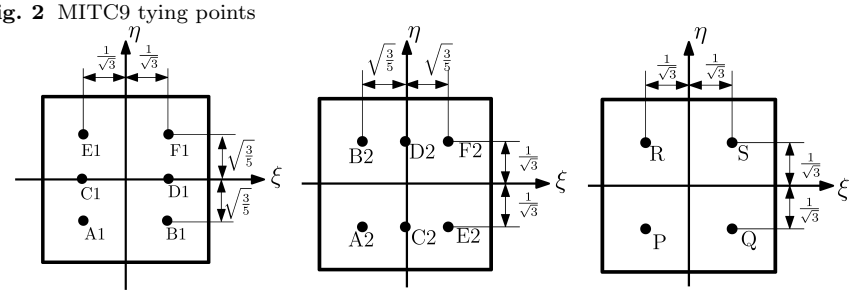

(a) Components of $\epsilon_{\alpha\alpha}$ and $\epsilon_{\alpha z}$ (b) Components of $\epsilon_{\beta\beta}$ and $\epsilon_{\beta z}$ (c) Components of $\epsilon_{\alpha\beta}$

Ω_k is the in-plane domain of a layer over the element and A_k is the thickness one. Via the constitutive equations, geometrical, MITC and CUF relations, the following governing equation reads

$$\boldsymbol{m}^k_{\tau isj}\ddot{\boldsymbol{u}}^k_{\tau i} + \boldsymbol{k}^k_{\tau sij}\boldsymbol{u}^k_{\tau i} = 0 \tag{14}$$

$\boldsymbol{k}^k_{\tau sij}$ and $\boldsymbol{m}^k_{\tau sij}$ are 3×3 matrices referred to as the fundamental nucleus of the stiffness and mass matrices, respectively. The components of the nuclei are given in [112]. The assembly over all nodes and elements and the introduction of the harmonic solution leads to the well-known eigenvalue problem,

$$(-\omega^2_n\boldsymbol{M} + \boldsymbol{K})\boldsymbol{U}_n = 0 \tag{15}$$

In CUF, the shell theory is a property of the node. In other words, each node can have a shell theory and the neighbour nodes others. In this work, the shell theory is the same for each node of an element and FSDT, and N=4 are the models adopted. Figure 3 shows an example of a shell mesh in which each element is either N=4 or FSDT. For more details on NDK, the reader may refer to [103,104]. NDK offers various options to deal with the edge nodes between elements with different theories. In this paper, the shared nodes have FSDT.

Fig. 3 Distribution of FSDT and fourth-order shell theories over a 2D mesh

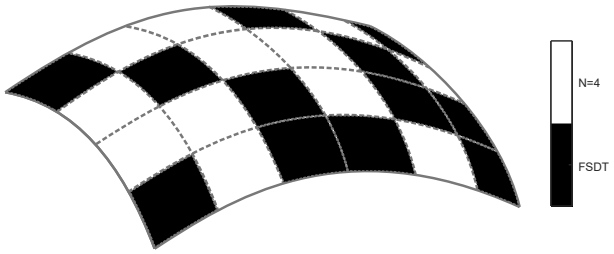

3 Axiomatic/asymptotic method and best theory distributions

The axiomatic/asymptotic method (AAM) is a methodology to assess the influence of generalized variables and the accuracy of structural models [105, 106]. In previous works, AAM acted on the set of variables of the expansion, e.g., in the case of N=4, AAM considered the fifteen primary variables and evaluated their influence. In the present paper, AAM acts on the distribution of shell theories over a given mesh. For instance, in the case of a 4×4 mesh, AAM evaluates the accuracy of every combination of FSDT and N=4, as shown in Fig. 3. Overall, 2^{16} mesh distributions are evaluated. The implementation of the AAM may follow various approaches; in this work:

1. Definition of parameters such as geometry, boundary conditions, materials, and layer layouts.
2. Axiomatic choice of a starting theory and definition of the starting nodal unknowns. Usually, the starting theory provides 3D-like solutions. The fourth-order, equivalent single layer shell model is the reference model of this paper.
3. Definition of a FEM mesh. In this work, a 4×4 mesh nine-node mesh was used as, for the considered problems, provides good accuracy.
4. The CUF generates the governing equations for the theory distributions considered.
5. For each structural theory distribution, the accuracy evaluation makes use of one or more control parameters; in this paper, the first ten natural frequencies.
6. The analysis is carried out multiple times to evaluate the relevance of problem parameters, e.g., thickness, orthotropic ratio, stacking sequence, boundary conditions.

Fig. 4 FE distributions in a 2D Cartesian reference frame and an example of BTD

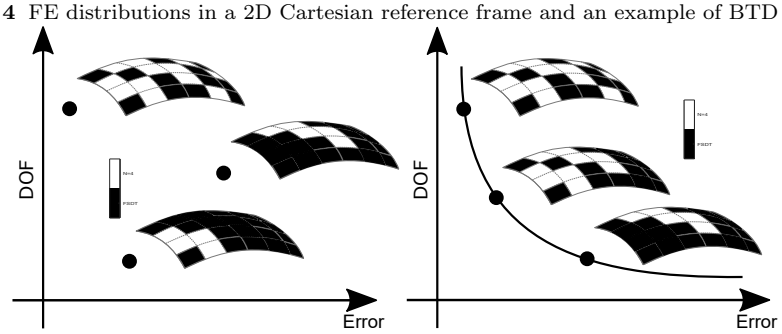

(a) Three shell theory distributions (b) Best Theory Distributions (BTD)

Two parameters can identify a distribution, namely, the number of DOF of the model and the error or accuracy provided. The use of two parameters allows the insertion of each FE distribution in a Cartesian reference frame,

as in Fig. 4a. The Best Theory Distribution (BTD) is the curve composed of all meshes with a given number of N=4 and FSDT elements providing the minimum error, see Fig. 4b. In the case of sixteen elements, the BTD will have sixteen models, the first one with all N=4 and the last one with all FSDT. To have a single error parameter, the BTD uses the average of the errors as follows:

$$Error = \sum_{i=1}^{10} \frac{f_i / f_i^{N=4}}{10} \tag{16}$$

Where f_i is the i-th frequency from a generic shell model, and $f_i^{N=4}$ is the one from the reference solution. As explained in the numerical result section, further control parameters, such as the standard deviation and the Modal Assurance Criterion (MAC), are useful to control the quality of the results.

4 Results

The numerical results consider spherical shells with geometrical and material characteristics retrieved from [26,113,108,22]. The shell can be obtained by considering a portion of a sphere with the following geometrical characteristics: a = b, $R_\alpha = R_\beta = R$, and R/a = 5. The material properties are $E_1/E_2 = 25$, $G_{12}/E_2 = G_{13}/E_2 = 0.5$, $G_{13}/E_2 = 0.2$, $\nu = 0.25$. The lamination angle is zero if aligned with β, and 90° if aligned with α. Two sets of geometrical boundary conditions were adopted, namely, simply-supported and clamped-free. The former acts on all four edges, in the latter, the edges parallel to α are clamped, and the others free. Unless otherwise stated, the focus is on symmetric modal shapes and the FE considers a quarter of shell. In all cases, a 4×4 mesh was used as in [108]. The analysis of symmetric modes allowed us to use a reduced number of elements via symmetric boundary conditions with a significant lower computational cost.

4.1 Simply-supported, 0/90/0

The first assessment deals with a simply-supported shell with symmetric lamination and various thickness ratios, a/h. Table 1 presents the first natural frequency from different models including higher- and first-order shear deformation theories, HSDT and FSDT, respectively, classical lamination theory, CLT, a layer-wise fourth-order model, LD4, and the present equivalent single layer full fourth-order expansion, N=4. The latter provides good accuracy if compared to LD4 and is set as the reference solution to build the BTD. Figure 5 shows the error given by each of the 2^{16} mesh combinations. The vertical axis reports the ratio between the total DOF of a given mesh and the total DOF in the case of the mesh with only fourth-order shell theories. The boundary values are D = 1, i.e., fifteen DOF per node and 1215 in total, and D = 0.333, i.e., five DOF per node and 405 overall. Figure 6 reports the mesh configurations

Table 1 0/90/0, a/h = 10, $\overline{\omega} = \omega\sqrt{\frac{\rho a^4}{h^2 E_T}}$

Model	
HSDT [26]	12.060
FSDT [25]	12.372
CLT [114]	15.233
LD4 [113]	11.685
N = 4	11.972

with the minimum error. The vertical axis reports the number of elements with the fourth-order shell theory and ranging from sixteen - all N=4 - to zero - all FSDT. The mesh distributions in the case of a/h = 100 are in Fig. 7. For the sake of brevity, just some of those distributions are reported in Fig. 8 for all the thickness ratios considered. Mesh distributions over one-quarter of the mesh and having four, eight and twelve elements with fourth-order kinematics are shown with the error, E, indicated in the captions. The bottom and left edges are those with the simply-supported boundary conditions applied. Such figures show where the higher-order kinematics is more relevant. In other words, considering four N=4 elements, the best configurations shown indicate the zones in which those elements are more necessary to minimize the error. Figure 9 reports MAC distributions obtained by averaging all those obtained by the mesh configurations in Fig. 6. The MAC values were obtained by using as reference the modal shapes from the full fourth-order model. The results

Fig. 5 All combinations for 0/90/0

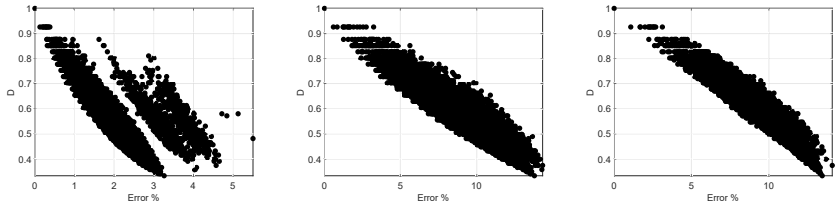

(a) a/h = 100 (b) a/h = 10 (c) a/h = 5

Fig. 6 BTD for 0/90/0

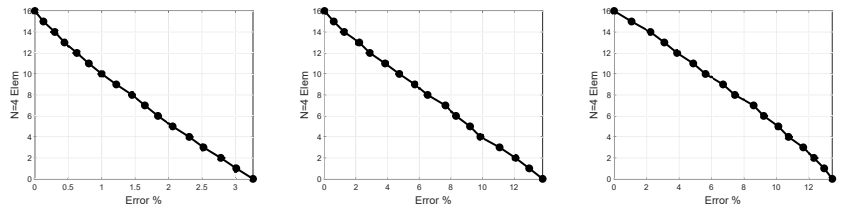

(a) a/h = 100 (b) a/h = 10 (c) a/h = 5

Fig. 7 Best theory distributions for 0/90/0, a/h = 100

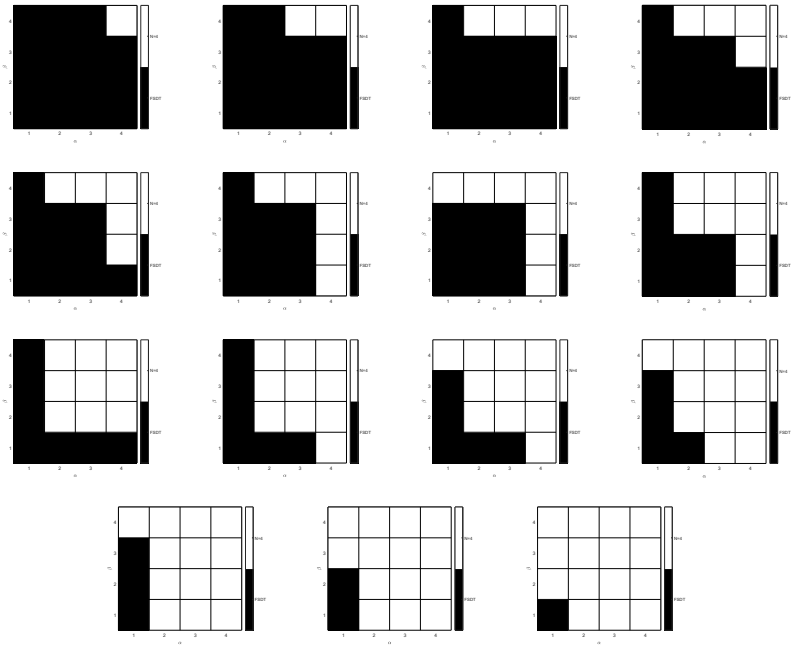

suggest the following:

- By considering all combinations of mesh distributions, the error range is higher than 5%, and, for thick shells, such a range increases significantly.
- The use of FSDT over the entire mesh provides acceptable errors in the case of thin shells only. The inclusion of a few fourth-order elements may be detrimental to the accuracy. Such an effect is very significant in the case of thin shells. The accuracy of FSDT could improve via more accurate shear correction factors. However, such factors strongly depend on the problem characteristics - shear stress distributions over the thickness, geometry, and modal shapes considered - and the order of the theory adopted. In other words, the calculation of these factors requires the use of refined models [115].
- The shell zones in which the fourth-order kinematics is more relevant depend on the thickness of the structure. In the case of thin shells, the higher-order models spread from the centre to the opposite corner. For thicker shells, the influence of the boundary conditions is more relevant, and higher-order kinematics appear along the simply-supported edges.
- The MAC distributions prove that the best mesh configurations detect the modal shapes with no significant accuracy losses.

Figures 10 and 11 show the results on the thin shell structure but without symmetry conditions; that is, the entire structure is considered to detect all

Fig. 8 Best theory distributions for 0/90/0

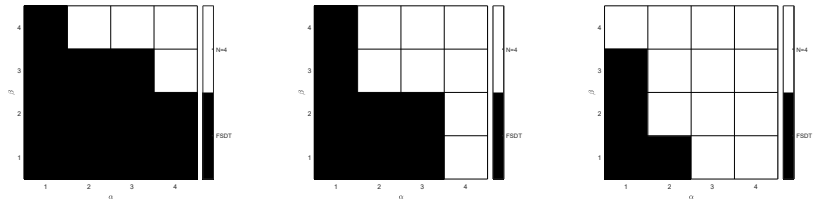

(a) a/h = 100, twelve FSDT, E=2.3 %

(b) a/h = 100, eight FSDT, E=1.5 %

(c) a/h = 100, four FSDT, E=0.6 %

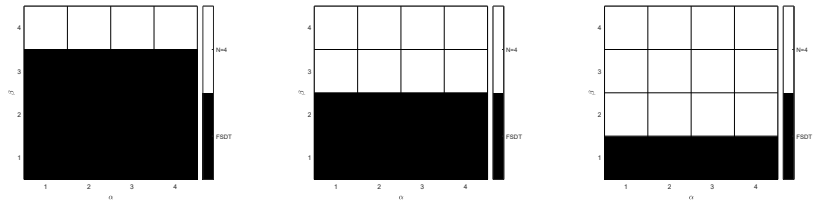

(d) a/h = 10, twelve FSDT, E=9.9 %

(e) a/h = 10, eight FSDT, E=6.5 %

(f) a/h = 10, four FSDT, E=2.9 %

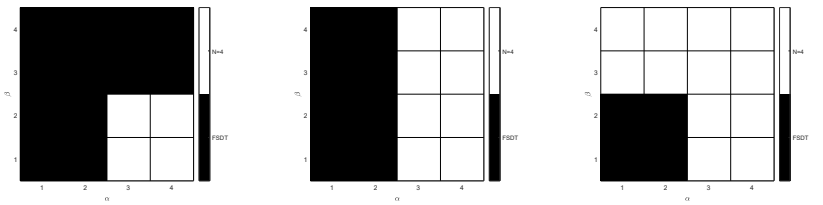

(g) a/h = 5, twelve FSDT, E=10.8 %

(h) a/h = 5, eight FSDT, E=7.4 %

(i) a/h = 5, four FSDT, E=3.9 %

Fig. 9 Averaged MAC for 0/90/0

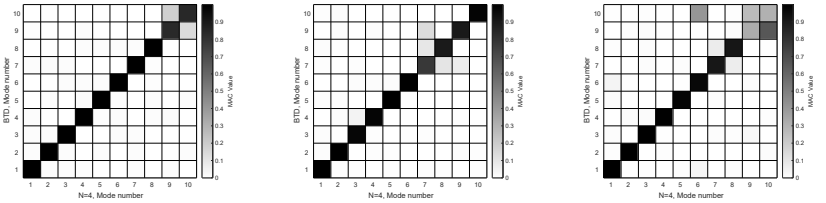

(a) a/h = 100

(b) a/h = 10

(c) a/h = 5

first ten modes. The results show that the error ranges are very similar to the previous case and the best mesh distributions follow the same patterns as before except for the last configuration in which, presumably, the presence of new modal shapes modifies the distribution. Given that no significant changes were found, all the subsequent assessments consider symmetric modes only.

Such a choice is due to the possibility of using a finer mesh and having a higher definition in the mesh distributions.

Fig. 10 BTD, all combinations, and MAC for 0/90/0, a/h = 100, all first ten modes

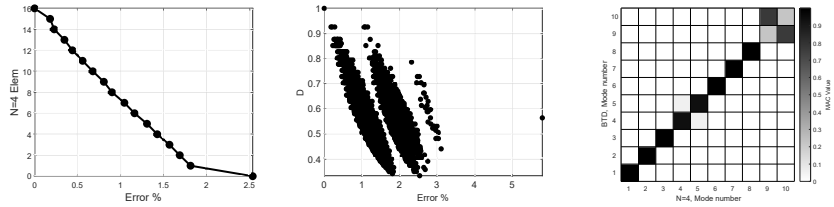

(a) BTD (b) All combinations (c) MAC

Fig. 11 Best theory distributions for 0/90/0, a/h = 100, all first ten modes

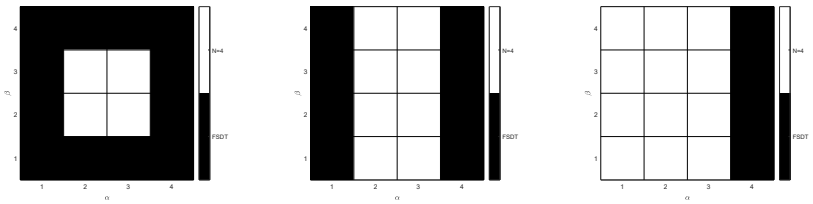

(a) a/h = 100, twelve FSDT, E=1.4 % (b) a/h = 100, eight FSDT, E=0.9 % (c) a/h = 100, four FSDT, E=0.4 %

4.2 Simply-supported, 0/90

The second shell configuration considers a different stacking sequence. All other parameters remain like those of the previous cases. Figure 12 shows all combinations and related errors, whereas Fig. 13 shows the best distributions. Selected mesh configurations are given in Fig. 14 and the MAC distributions in Fig. 15.

The analysis of the results suggests that

- The accuracy distributions lie within similar ranges as compared to the previous numerical case. However, in the thin case, misplaced refined models may be more detrimental than in the 0/90/0.
- The patterns followed by the higher-order kinematics over the mesh present a more significant influence of the external edges.
- The MAC distributions have some non-diagonal terms, but the overall match is good.

Fig. 12 All combinations for 0/90

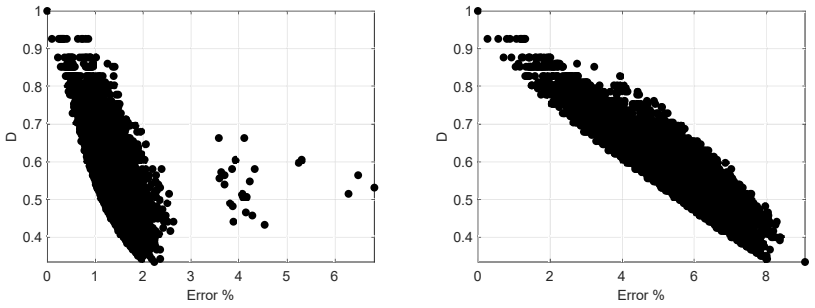

(a) a/h = 100 (b) a/h = 10

Fig. 13 BTD for 0/90

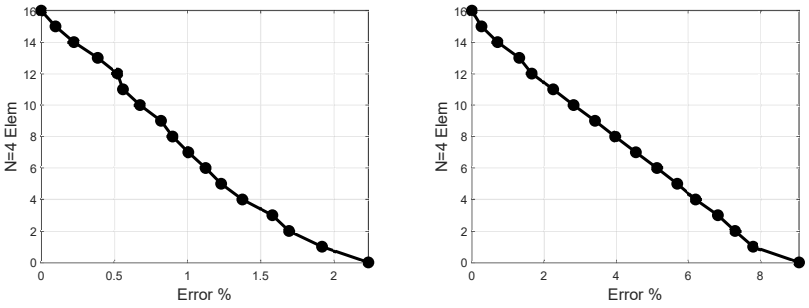

(a) a/h = 100 (b) a/h = 10

4.3 Clamped-free, 0/90/0

The last assessment considers a different set of boundary conditions in which the top and bottom edges are clamped and the lateral ones free. All the other features of the problem remain as in the previous cases. The results are provided in Figs. 16, 17, 18, 19. The results confirm the predominant role of the boundary conditions and the thickness in the determination of the best mesh distribution. In the thin case, the higher-order theories are needed far from the geometrical boundary conditions. On the other hands, in the thicker cases, the influence of the geometrical boundary conditions is evident.

5 Conclusion

This paper has presented a new methodology to determine the most critical areas of given shell problems by providing the best distributions of refined shell theories over the FE mesh. The methodology makes use of CUF for governing equations, the NDK to distribute different shell theories node-wise,

Fig. 14 Best theory distributions for 0/90

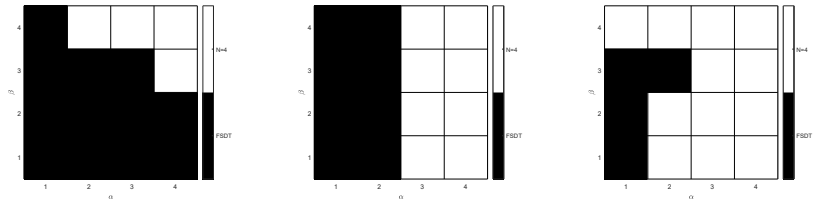

(a) a/h = 100, twelve FSDT, E=1.4 %

(b) a/h = 100, eight FSDT, E=0.9 %

(c) a/h = 100, four FSDT, E=0.5 %

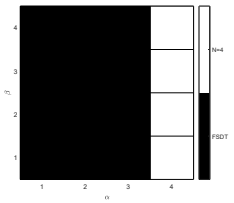

(d) a/h = 10, twelve FSDT, E=6.2 %

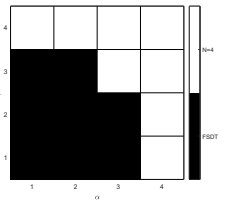

(e) a/h = 10, eight FSDT, E=4.0 %

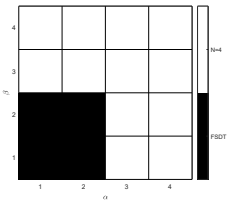

(f) a/h = 10, four FSDT, E=1.7 %

Fig. 15 Averaged MAC for 0/90

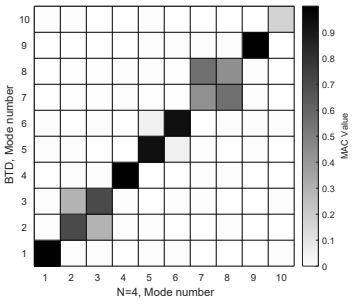

(a) a/h = 100

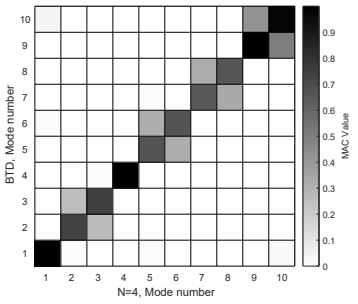

(b) a/h = 10

and the AAM to evaluate the accuracy. The numerical results focused on the free vibration analyses and assessed various shell configurations concerning boundary conditions, thickness and lamination. The main findings are the following:

- The thickness of the structure and the boundary conditions are the leading features to establish the most critical areas.
- For thin shells, the areas demanding the use of refined models are far from the geometrical boundary conditions. For thick shells, on the other hand, the vicinity of boundary conditions is a more significant indicator.
- The use of asymmetric laminations makes the influence of boundary conditions greater.

Fig. 16 All combinations, clamped-free

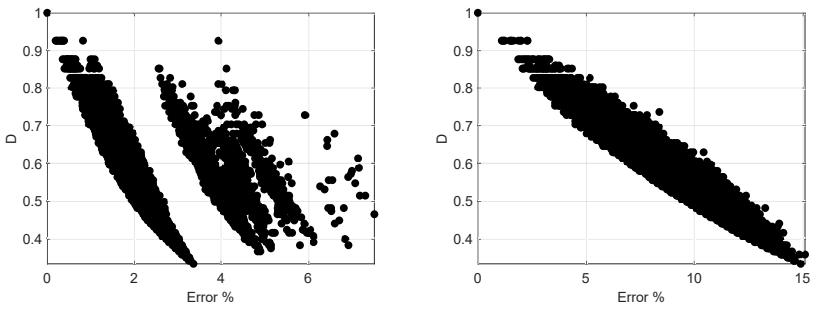

(a) 0/90/0, a/h = 100 (b) 0/90/0, a/h = 20

Fig. 17 BTD, clamped-free

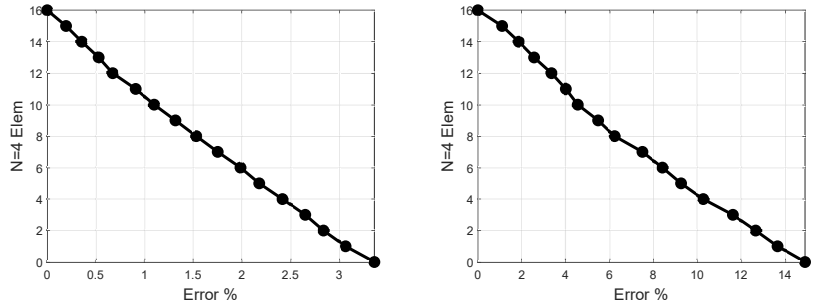

(a) 0/90/0, a/h = 100 (b) 0/90/0, a/h = 20

– The accuracy of the various mesh distributions can change significantly. For thick, shells, in particular, errors higher than 10% may show up.

The approach presented in this paper can be further extended to consider more complex configurations and aiming at providing guidelines for the structural modelling of engineering structures. To this purpose, the use of machine learning techniques represents a viable way as the methodology presented has good coding capabilities and the generation of data for deep-learning is feasible with low computational costs.

Conflict of interest

On behalf of all authors, the corresponding author states that there is no conflict of interest.

Fig. 18 Best theory distributions, clamped-free

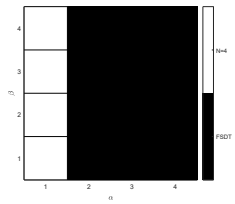

(a) 0/90/0, a/h = 100, twelve FSDT, E=2.4 %

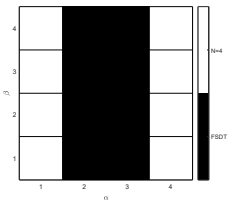

(b) 0/90/0, a/h = 100, eight FSDT, E=1.5 %

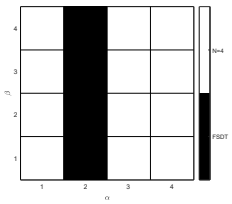

(c) 0/90/0, a/h = 100, four FSDT, E=0.7 %

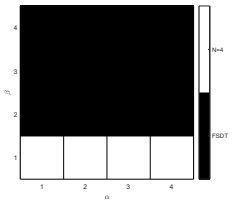

(d) 0/90/0, a/h = 20, twelve FSDT, E=10.3 %

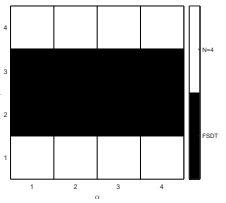

(e) 0/90/0, a/h = 20, eight FSDT, E=6.2 %

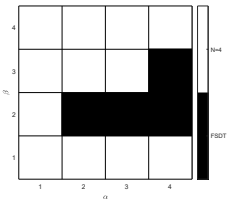

(f) 0/90/0, a/h = 20, four FSDT, E=3.4 %

Fig. 19 Averaged MAC for 0/90/0, clamped-free

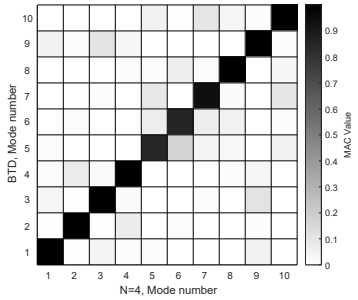

(a) 0/90/0, a/h = 100

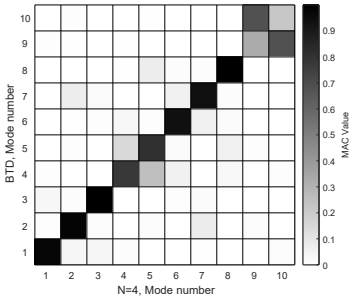

(b) 0/90/0, a/h = 20

References

1. A. L. Cauchy. Sur l'équilibre et le mouvement d'une plaque solide. *Exercises de Matematique*, 3:328–355, 1828.
2. S. D. Poisson. Memoire sur l'équilibre et le mouvement des corps elastique. *Mem. Acad. Sci.*, 1829.
3. A.E.H. Love. *The Mathematical Theory of Elasticity*. Cambridge Univ Press, fourth edition, 1927.
4. G. Kirchhoff. Uber das gleichgewicht und die bewegung einer elastischen scheibe. *Journal fur reins und angewandte Mathematik*, 40:51–88, 1850.
5. E. Reissner. The effect of transverse shear deformation on the bending of elastic plates. *Journal of Applied Mechanics*, 12:69–76, 1945.
6. R.D. Mindlin. Influence of rotatory inertia and shear in flexural motions of isotropic elastic plates. *Journal of Applied Mechanics*, 18:1031–1036, 1951.

7. S.A. Ambartsumian. Nontraditional theories of shells and plates. *Applied Mechanics Reviews*, 55(5):R35–R44, 2002.
8. E. Carrera. Theories and finite elements for multilayered, anisotropic, composite plates and shells. *Archives of Computational Methods in Engineering*, 9(2):87–140, 2002.
9. S.G. Lekhnitskii. Strength calculation of composite beams. *Vestnik inzhen i tekhnikov*, 9, 1935.
10. F.B. Hildebrand, E. Reissner, and G.B. Thomas. Notes on the foundations of the theory of small displacements of orthotropic shells. *NACA TN-1833*, 1949.
11. W.T. Koiter. A consistent first approximation in the general theory of thin elastic shells. *Proceedings of Symposium on the Theory of Thin Elastic Shells, August 1959, North-Holland, Amsterdam*, pages 12–23, 1959.
12. S.A. Ambartsumian. Contributions to the theory of anisotropic layered shells. *Applied Mechanics Reviews*, 15:245–249, 1962.
13. N.J. Pagano. Exact solutions for composite laminates in cylindrical bending. *Journal of Composite Materials*, 3(3):398–411, 1969.
14. A.W. Leissa. Vibration of shells. *NASA-SP-288*, LC-77-186367, 1973.
15. E.I. Grigolyuk and G.M. Kulikov. General directions of the development of theory of shells. *Mechanics of Composite Materials*, 24(287–298), 1988.
16. K. Kapania. A review on the analysis of laminated shells. *ASME Journal of Pressure Vessel Technology*, 111(2):88–96, 1989.
17. A.K. Noor and W.S. Burton. Assessment of computational models for multilayered composite shells. *Applied Mechanics Reviews*, 43(4):67–97, 1989.
18. M. Touratier. A generalization of shear deformation theories for axisymmetric multilayered shells. *International Journal of Solids and Structures*, 29(11):1379 – 1399, 1992.
19. V.V. Vasil'Ev and S.A. Lur'E. On refined theories of beams, plates, and shells. *Journal of Composite Materials*, 26(4):546–557, 1992.
20. J. N. Reddy and D. H. Robbins. Theories and computational models for composite laminates. *Applied Mechanics Reviews*, 47(6):147–165, 1994.
21. E. Carrera. A study of transverse normal stress effect on vibration of multilayered plates and shells. *Journal of Sound and Vibration*, 225(5):803 – 829, 1999.
22. M. Petrolo and E. Carrera. Methods and guidelines for the choice of shell theories. *Acta Mechanica*, 231:395–434, 2020.
23. M. Qatu. Recent research advances in the dynamic behavior of shells: 1989-2000, part 1: Laminated composite shells. *Applied Mechanics Review*, 55(4):325–350, 2002.
24. M. Qatu, R.W. Sullivan, and W. Wang. Recent research advances on the dynamic analysis of composite shells: 2000–2009. *Composite Structures*, 93(1):14 – 31, 2010.
25. J.N. Reddy. Exact solutions of moderately thick laminated shells. *Journal of Engineering Mechanics*, 110(5):794–809, 1984.
26. J.N. Reddy and C.F. Liu. A higher-order shear deformation theory of laminated elastic shells. *International Journal of Engineering Science*, 23(3):319 – 330, 1985.
27. R.K. Khare, V. Rode, A.K. Garg, and S.P. John. Higher-order closed-form solutions for thick laminated sandwich shells. *Journal of Sandwich Structures & Materials*, 7(4):335–358, 2005.
28. A.K. Garg, R.K. Khare, and T. Kant. Higher-order closed-form solutions for free vibration of laminated composite and sandwich shells. *Journal of Sandwich Structures & Materials*, 8(3):205–235, 2006.
29. H. Biglari and A.A. Jafari. High-order free vibrations of doubly-curved sandwich panels with flexible core based on a refined three-layered theory. *Composite Structures*, 92(11):2685 – 2694, 2010.
30. E. Asadi, W. Wang, and M.S. Qatu. Static and vibration analyses of thick deep laminated cylindrical shells using 3d and various shear deformation theories. *Composite Structures*, 94(2):494 – 500, 2012.
31. S. Hosseini-Hashemi, S.R. Atashipour, M. Fadaee, and U.A. Girhammar. An exact closed-form procedure for free vibration analysis of laminated spherical shell panels based on Sanders theory. *Archive of Applied Mechanics*, 82(7):985–1002, 2012.
32. J.L. Mantari and C. Guedes Soares. Analysis of isotropic and multilayered plates and shells by using a generalized higher-order shear deformation theory. *Composite Structures*, 94(8):2640 – 2656, 2012.

33. C. Hwu, H.W. Hsu, and Y.H. Lin. Free vibration of composite sandwich plates and cylindrical shells. *Composite Structures*, 171:528 – 537, 2017.
34. G. Jin, T. Ye, X. Ma, Y. Chen, Z. Su, and X. Xie. A unified approach for the vibration analysis of moderately thick composite laminated cylindrical shells with arbitrary boundary conditions. *International Journal of Mechanical Sciences*, 75:357 – 376, 2013.
35. G. Jin, T. Ye, Y. Chen, Z. Su, and Y. Yan. An exact solution for the free vibration analysis of laminated composite cylindrical shells with general elastic boundary conditions. *Composite Structures*, 106:114 – 127, 2013.
36. T. Ye, G. Jin, Y. Chen, X. Ma, and Z. Su. Free vibration analysis of laminated composite shallow shells with general elastic boundaries. *Composite Structures*, 106:470 – 490, 2013.
37. Y. Qu and G. Meng. Dynamic analysis of composite laminated and sandwich hollow bodies of revolution based on three-dimensional elasticity theory. *Composite Structures*, 112:378 – 396, 2014.
38. G. Jin, T. Ye, and S. Shi. Three-dimensional vibration analysis of isotropic and orthotropic open shells and plates with arbitrary boundary conditions. *Shock and Vibration*, 2015, 2015.
39. H. Li, F. Pang, X. Wang, Y. Du, and H. Chen. Free vibration analysis for composite laminated doubly-curved shells of revolution by a semi analytical method. *Composite Structures*, 201:86 – 111, 2018.
40. R. Zhong, J. Tang, A. Wang, C. Shuai, and Q. Wang. An exact solution for free vibration of cross-ply laminated composite cylindrical shells with elastic restraint ends. *Computers and Mathematics with Applications*, 77(3):641 – 661, 2019.
41. A.L. Poore, A. Barut, and E. Madenci. Free vibration of laminated cylindrical shells with a circular cutout. *Journal of Sound and Vibration*, 312(1):55 – 73, 2008.
42. M. Shakouri and M.A. Kouchakzadeh. Analytical solution for vibration of generally laminated conical and cylindrical shells. *International Journal of Mechanical Sciences*, 131-132:414 – 425, 2017.
43. S.G.P. Castro and M.V. Donadon. Assembly of semi-analytical models to address linear buckling and vibration of stiffened composite panels with debonding defect. *Composite Structures*, 160:232 – 247, 2017.
44. M.H. Kargarnovin and M. Hashemi. Free vibration analysis of multilayered composite cylinder consisting fibers with variable volume fraction. *Composite Structures*, 94(3):931 – 944, 2012.
45. A.V. Lopatin and E.V. Morozov. Fundamental frequency of the laminated composite cylindrical shell with clamped edges. *International Journal of Mechanical Sciences*, 92:35 – 43, 2015.
46. M. Nasihatgozar, S.M.R. Khalili, and K.M. Fard. General equations for free vibrations of thick doubly curved sandwich panels with compressible and incompressible core using higher order shear deformation theory. *Steel and Composite Structures*, 24(2):151–176, 2017.
47. C.P. Wu and K.H. Chiu. Rmvt-based meshless collocation and element-free galerkin methods for the quasi-3d free vibration analysis of multilayered composite and fgm plates. *Composite Structures*, 93(5):1433 – 1448, 2011.
48. A.H. Sofiyev. Application of the first order shear deformation theory to the solution of free vibration problem for laminated conical shells. *Composite Structures*, 188:340 – 346, 2018.
49. A.V. Singh and V. Kumar. Vibration of laminated shallow shells on quadrangular boundary. *Journal of Aerospace Engineering*, 9(2):52–57, 1996.
50. A.V. Singh and L. Shen. Free vibration of open circular cylindrical composite shells with point supports. *Journal of Aerospace Engineering*, 18(2):120–128, 2005.
51. X. Zhao, K.M. Liew, and T.Y. Ng. Vibration analysis of laminated composite cylindrical panels via a meshfree approach. *International Journal of Solids and Structures*, 40(1):161 – 180, 2003.
52. T. Ye, G. Jin, Z. Su, and X. Jia. A unified Chebyshev–Ritz formulation for vibration analysis of composite laminated deep open shells with arbitrary boundary conditions. *Archive of Applied Mechanics*, 84:441–471, 2017.

53. G. Jin, T. Ye, X. Jia, and S. Gao. A general Fourier solution for the vibration analysis of composite laminated structure elements of revolution with general elastic restraints. *Composite Structures*, 109:150 – 168, 2014.
54. X. Song, Q. Han, and J. Zhai. Vibration analyses of symmetrically laminated composite cylindrical shells with arbitrary boundaries conditions via Rayleigh–Ritz method. *Composite Structures*, 134:820 – 830, 2015.
55. F. Pang, H. Li, H. Chen, and Y. Shan. Free vibration analysis of combined composite laminated cylindrical and spherical shells with arbitrary boundary conditions. *Mechanics of Advanced Materials and Structures*, 2019.
56. G. Jin, Z. Su, T. Ye, and X. Jia. Three-dimensional vibration analysis of isotropic and orthotropic conical shells with elastic boundary restraints. *International Journal of Mechanical Sciences*, 89:207 – 221, 2014.
57. C. Yang, G. Jin, Y. Zhang, and Z. Liu. A unified three-dimensional method for vibration analysis of the frequency-dependent sandwich shallow shells with general boundary conditions. *Applied Mathematical Modelling*, 66:59 – 76, 2019.
58. A.V. Singh. Free vibration analysis of deep doubly curved sandwich panels. *Computers and Structures*, 73(1):385 – 394, 1999.
59. M. Hemmatnezhad, G.H. Rahimi, M. Tajik, and F. Pellicano. Experimental, numerical and analytical investigation of free vibrational behavior of GFRP-stiffened composite cylindrical shells. *Composite Structures*, 120:509 – 518, 2015.
60. X. Xie, H. Zheng, and G. Jin. Integrated orthogonal polynomials based spectral collocation method for vibration analysis of coupled laminated shell structures. *International Journal of Mechanical Sciences*, 98:132 – 143, 2015.
61. Y. Qu, H. Hua, and G. Meng. A domain decomposition approach for vibration analysis of isotropic and composite cylindrical shells with arbitrary boundaries. *Composite Structures*, 95:307 – 321, 2013.
62. Y. Qu, X. Long, S. Wu, and G. Meng. A unified formulation for vibration analysis of composite laminated shells of revolution including shear deformation and rotary inertia. *Composite Structures*, 98:169 – 191, 2013.
63. J. Guo, D. Shi, Q. Wang, J. Tang, and C. Shuai. Dynamic analysis of laminated doubly-curved shells with general boundary conditions by means of a domain decomposition method. *International Journal of Mechanical Sciences*, 138-139:159 – 186, 2018.
64. A. Alibeigloo. Static and vibration analysis of axi-symmetric angle-ply laminated cylindrical shell using state space differential quadrature method. *International Journal of Pressure Vessels and Piping*, 86(11):738 – 747, 2009.
65. H.V. Lakshminarayana and K. Dwarakanath. Free vibration characteristics of cylindrical shells made of composite materials. *Journal of Sound and Vibration*, 154(3):431 – 439, 1992.
66. J. Zhu. Free vibration analysis of multilayered composite plates and shells with the natural approach. *Computer Methods in Applied Mechanics and Engineering*, 130(1):133 – 149, 1996.
67. N.S. Bardell, J.M. Dunsdon, and R.S. Langley. Free and forced vibration analysis of thin, laminated, cylindrically curved panels. *Composite Structures*, 38(1):453 – 462, 1997.
68. T. Park, K. Kim, and S. Han. Linear static and dynamic analysis of laminated composite plates and shells using a 4-node quasi-conforming shell element. *Composites Part B: Engineering*, 37(2):237 – 248, 2005.
69. H. Nguyen-Van, N. Mai-Duy, and T. Tran-Cong. Free vibration analysis of laminated plate/shell structures based on fsdt with a stabilized nodal-integrated quadrilateral element. *Journal of Sound and Vibration*, 313(1):205 – 223, 2008.
70. H. Nguyen-Van, N. Mai-Duy, W. Karunasena, and T. Tran-Cong. Buckling and vibration analysis of laminated composite plate/shell structures via a smoothed quadrilateral flat shell element with in-plane rotations. *Computers and Structures*, 89(7):612 – 625, 2011.
71. D. Chakravorty, J.N. Bandyopadhyay, and P.K. Sinha. Finite element free vibration analysis of point supported laminated composite cylindrical shells. *Journal of Sound and Vibration*, 181(1):43 – 52, 1995.
72. K.S.S. Ram and T.S. Babu. Free vibration of composite spherical shell cap with and without a cutout. *Computers and Structures*, 80(23):1749 – 1756, 2002.

73. S.C. Han, S. Choi, and S.Y. Chang. Nine-node resultant-stress shell element for free vibration and large deflection of composite laminates. *Journal of Aerospace Engineering*, 19(2):103–120, 2006.
74. S. Jayasankar, S. Mahesh, S. Narayanan, and C. Padmanabhan. Dynamic analysis of layered composite shells using nine node degenerate shell elements. *Journal of Sound and Vibration*, 299(1):1 – 11, 2007.
75. R.K. Khare, T. Kant, and A.K. Garg. Free vibration of composite and sandwich laminates with a higher-order facet shell element. *Composite Structures*, 65(3):405 – 418, 2004.
76. R.K. Khare, A.K. Garg, and T. Kant. Free vibration of sandwich laminates with two higher-order shear deformable facet shell element models. *Journal of Sandwich Structures & Materials*, 7(3):221–244, 2005.
77. A. Kumar, P. Bhargava, and A. Chakrabarti. Vibration of laminated composite skew hypar shells using higher order theory. *Thin-Walled Structures*, 63:82 – 90, 2013.
78. S.N. Thakur and C. Ray. An accurate C0 finite element model of moderately thick and deep laminated doubly curved shell considering cross sectional warping. *Thin-Walled Structures*, 94:384 – 393, 2015.
79. W.H. Lee and S.C. Han. Free and forced vibration analysis of laminated composite plates and shells using a 9-node assumed strain shell element. *Computational Mechanics*, 39(1):41–58, 2006.
80. D. Chronopoulos, M. Ichchou, B. Troclet, and O. Bareille. Efficient prediction of the response of layered shells by a dynamic stiffness approach. *Composite Structures*, 97:401 – 404, 2013.
81. D. He, D. Shi, Q. Wang, and C. Shuai. Wave based method (wbm) for free vibration analysis of cross-ply composite laminated cylindrical shells with arbitrary boundaries. *Composite Structures*, 213:284 – 298, 2019.
82. X. Xie, G. Jin, Y. Yan, S.X. Shi, and Z. Liu. Free vibration analysis of composite laminated cylindrical shells using the haar wavelet method. *Composite Structures*, 109:169 – 177, 2014.
83. X. Xie, G. Jin, W. Li, and Z. Liu. A numerical solution for vibration analysis of composite laminated conical, cylindrical shell and annular plate structures. *Composite Structures*, 111:20 – 30, 2014.
84. O. Civalek. Numerical analysis of free vibrations of laminated composite conical and cylindrical shells: Discrete singular convolution (dsc) approach. *Journal of Computational and Applied Mathematics*, 205(1):251 – 271, 2007.
85. O. Civalek. Vibration analysis of laminated composite conical shells by the method of discrete singular convolution based on the shear deformation theory. *Composites Part B: Engineering*, 45(1):1001 – 1009, 2013.
86. K.K. Viswanathan, S. Javed, K. Prabakar, Z.A. Aziz, and I.A. Bakar. Free vibration of anti-symmetric angle-ply laminated conical shells. *Composite Structures*, 122:488 – 495, 2015.
87. Q. Wang, D. Shao, and B. Qin. A simple first-order shear deformation shell theory for vibration analysis of composite laminated open cylindrical shells with general boundary conditions. *Composite Structures*, 184:211 – 232, 2018.
88. A.K. Noor, W.S. Burton, and J.M. Peters. Predictor-corrector procedures for stress and free vibration analyses of multilayered composite plates and shells. *Computer Methods in Applied Mechanics and Engineering*, 82(1):341 – 363, 1990.
89. R.A. Chaudhuri and H.R.H. Kabir. Effect of boundary constraint on the frequency response of moderately thick doubly curved cross-ply panels using mixed Fourier solution functions. *Journal of Sound and Vibration*, 283(1):263 – 293, 2005.
90. O. Rahmani, S.M.R. Khalili, and K. Malekzadeh. Free vibration response of composite sandwich cylindrical shell with flexible core. *Composite Structures*, 92(5):1269 – 1281, 2010.
91. S.M.R. Khalili, S. Tafazoli, and K.M. Fard. Free vibrations of laminated composite shells with uniformly distributed attached mass using higher order shell theory including stiffness effect. *Journal of Sound and Vibration*, 330(26):6355 – 6371, 2011.
92. S.N. Thakur, C. Ray, and S. Chakraborty. A new efficient higher-order shear deformation theory for a doubly curved laminated composite shell. *Acta Mechanica*, 228(1):69–87, 2017.

93. S.N. Thakur, C. Ray, and S. Chakraborty. Response sensitivity analysis of laminated composite shells based on higher-order shear deformation theory. *Archive of Applied Mechanics*, 88(8):1429–1459, 2018.
94. A. Dasgupta and K.H. Huang. A layer-wise analysis for free vibrations of thick composite spherical panels. *Journal of Composite Materials*, 31(7):658–671, 1997.
95. P. Malekzadeh, M. Farid, and P. Zahedinejad. A three-dimensional layerwise-differential quadrature free vibration analysis of laminated cylindrical shells. *International Journal of Pressure Vessels and Piping*, 85(7):450 – 458, 2008.
96. M. Yaqoob Yasin and S. Kapuria. An efficient layerwise finite element for shallow composite and sandwich shells. *Composite Structures*, 98:202 – 214, 2013.
97. K. Khan, B.P. Patel, and Y. Nath. Dynamic characteristics of bimodular laminated panels using an efficient layerwise theory. *Composite Structures*, 132:759 – 771, 2015.
98. M. Marjanović and D. Vuksanović. Free vibrations of laminated composite shells using the rotation-free plate elements based on reddy's layerwise discontinuous displacement model. *Composite Structures*, 156:320 – 332, 2016.
99. A. Kumar, A. Chakrabarti, and P. Bhargava. Vibration of laminated composites and sandwich shells based on higher order zigzag theory. *Engineering Structures*, 56:880 – 888, 2013.
100. C. Lee and D.H. Hodges. Dynamic variational-asymptotic procedure for laminated composite shells—part I: Low-frequency vibration analysis. *Journal of Applied Mechanics*, 76(1), 2008.
101. A. Louhghalam, T. Igusa, and M. Tootkaboni. Dynamic characteristics of laminated thin cylindrical shells: Asymptotic analysis accounting for edge effect. *Composite Structures*, 112:22 – 37, 2014.
102. E. Carrera. Theories and finite elements for multilayered plates and shells: a unified compact formulation with numerical assessment and benchmarking. *Archives of Computational Methods in Engineering*, 10(3):216–296, 2003.
103. E. Carrera, A. Pagani, and S. Valvano. Shell elements with through-the-thickness variable kinematics for the analysis of laminated composite and sandwich structures. *Composites Part B: Engineering*, 111:294 – 314, 2017.
104. G. Li, E. Carrera, M. Cinefra, A.G. de Miguel, A. Pagani, and E. Zappino. An adaptable refinement approach for shell finite element models based on node-dependent kinematics. *Composite Structures*, 210:1 – 19, 2019.
105. E. Carrera and M. Petrolo. Guidelines and recommendation to construct theories for metallic and composite plates. *AIAA Journal*, 48(12):2852–2866, 2010.
106. E. Carrera and M. Petrolo. On the effectiveness of higher-order terms in refined beam theories. *Journal of Applied Mechanics*, 78, 2011.
107. E. Carrera, M. Cinefra, A. Lamberti, and M. Petrolo. Results on best theories for metallic and laminated shells including layer-wise models. *Composite Structures*, 126:285–298, 2015.
108. M. Petrolo and E. Carrera. Best theory diagrams for multilayered structures via shell finite elements. *Advanced Modeling and Simulation in Engineering Science*, 6(4):1–23, 2019.
109. E. Carrera, F. Miglioretti, and M. Petrolo. Computations and evaluations of higher-order theories for free vibration analysis of beams. *Journal of Sound and Vibration*, 331(19):4269 – 4284, 2012.
110. J.N. Reddy. *Mechanics of laminated composite plates and shells. Theory and Analysis.* CRC Press, 2^{nd} edition, 2004.
111. K.J. Bathe and E.N. Dvorkin. A formulation of general shell elements—the use of mixed interpolation of tensorial components. *International Journal for Numerical Methods in Engineering*, 22(3):697–722, 1986.
112. E. Carrera, M. Cinefra, M. Petrolo, and E. Zappino. *Finite Element Analysis of Structures through Unified Formulation.* John Wiley & Sons, Chichester, 2014.
113. M. Cinefra. Free-vibration analysis of laminated shells via refined MITC9 elements. *Mechanics of Advanced Materials and Structures*, 23(9):937–947, 2016.
114. E. Carrera. The effects of shear deformation and curvature on buckling and vibrations of cross-ply laminated composite shells. *Journal of Sound and Vibrations*, 150(3):405–433, 1991.

115. E. Carrera, M. Petrolo, and E. Zappino. Performance of CUF approach to analyze the structural behavior of slender bodies. *Journal of Structural Engineering*, 138(2):285–297, 2012.